JOURNAL OF SOLID STATE CHEMISTRY **136,** 34–45 (1998)
ARTICLE NO. SC977644

Synthesis, Crystal Structure, Infrared Characterization, and Electrical Properties of the New $Bi_9(V_{1-x}P_x)_2ClO_{18}$ Series ($0 \leq x \leq 1$)

O. Mentre and F. Abraham

Laboratoire de Cristallochimie et Physicochimie du Solide URA, CNRS 452, Ecole Nationale Supérieure de Chimie de Lille, Université des Sciences et Technologies de Lille, B.P. 108, 59652 Villeneuve d'Ascq Cedex, France

Received June 11, 1997; in revised form September 30, 1997; accepted October 4, 1997

A new series of oxyhalides of formula $Bi_9(V_{1-x}P_x)_2ClO_{18}$ has been synthesized and characterized. Single crystals of the vanadate end of the series were prepared under an oxygen pressure obtained from the thermal decomposition of $KClO_3$ acting on a $V-Bi_2O_3$ mixture. $Bi_9V_2ClO_{18}$ crystallizes in the $P2_1/m$ space group with unit cell parameters $a = 11.671(2)$ Å, $b = 5.463(1)$ Å, $c = 14.792(3)$ Å, and $\beta = 93.67(1)^\circ$. Its crystal structure consists of a very complex linkage of bismuth oxychloropolyhedra connected to orthovanadate tetrahedra. It somewhat releases sections of square planes of oxygen with bismuth, alternately located on and below the planes, similar to the $(Bi_2O_2)^{2+}$ layers of the Aurivillius phases. The most significant feature of the tridimensional framework is the existence of large tunnels with elliptical cross sections parallel to the b axis and occupied by the underbonded Cl^- anions. Conductivity measurements performed on our samples indicate an ionic mobility assigned to chloride motion. This mobility decreases when VO_4^{3-} are replaced with PO_4^{3-}. This phenomenon is related to the decrease in tunnel cross section on substitution and confirms the role of Cl^- in the conductivity process. To better characterize our compounds, we carried out an infrared study of the solid solution. This study revealed that $P-O$ bonds are stronger than $V-O$ bonds. A factor group analysis was achieved using our crystallographic data.

INTRODUCTION

Ever since our discovery of high ionic conductivity in $Bi_4V_2O_{11}$ (1), interest in materials containing both bismuth and vanadium has greatly increased. The structure of $Bi_4V_2O_{11}$ derives from the Aurivillius type, where $(Bi_2O_2)^{2+}$ layers alternate with perovskite slabs of composition $[VO_{3.5}\square_{0.5}]^{2-}$ (2, 3). Numerous metals have been successfully substituted for vanadium in $Bi_4V_2O_{11}$ and been found to improve the conductivity properties, leading to the Bimevox family (2, 4). On the other hand, new bismuth mixed-valence vanadium oxides have recently been synthesized. Joubert *et al.* (5) prepared $Bi_6V_3O_{16}$ (or $Bi_4V_2O_{10.67}$), a mixed-valence Aurivillius type compound where $(Bi_2O_2)^{2+}$ layers are interleaved with $(V_3O_{10})^{2-}$ ribbons build up from one V(IV) octahedron and two V(V) tetrahedra. For the same Bi/V ratio, Galy *et al.* (6) prepared a vanadium oxide bronze, an Aurivillius type $Bi_4V^{5+}_{2-2x}V^{4+}_{2x}O_{11-x}$; the more reduced vanadium oxide $Bi_4V_2O_{10}$ ($x = 1$) contains $(V_2O_6)_n$ layers of corner-sharing $V^{4+}O_5$ square pyramids between $(Bi_2O_2)^{2+}$ layers. Ramanan *et al.* (7) studied $Bi_2V_3O_9$, a vanadium(IV) bismuth oxide with a distorted pyrochlore structure; this compound is in fact a mixture of a partially reduced Aurivillius phase and $Bi_{1.7}V_8O_{16}$, a new bismuth mixed-valence vanadium oxide with a hollandite-type structure (8). With the aim of growing single crystals of partially reduced $Bi_4V_2O_{11}$ or of new mixed-valence vanadium oxides of bismuth, a study of several Bi_2O_3–V–$KClO_3$ mixtures has been undertaken. The efficiency of using $KClO_3$, acting both as an oxidizing agent and as a flux from molten KCl to grow single crystals of partially oxidized transition metal oxides, has already been demonstrated; for example, intermediate oxidation degrees have been stabilized for ruthenium or osmium in $La_3Ru_3O_{11}$ (9), $La_4M_6O_{19}$ (M = Ru, Os) (10), and $La_{3.5}Ru_4O_{13}$ (11). A serious disadvantage of growing crystals from a flux is that the crystals may contain traces of the salt. In our reaction, chloride ions were introduced in the compound obtained, leading to the preparation of an oxyhalide vanadate of bismuth. This type of compound is still of current interest, especially for some diversified structural features, justifying the recent work on the new oxychlorovanadate $Ln_3VO_4Cl_6$ (L = La, Ce, Pr, Nd) (12) or the recently prepared newly distorted variants of the Sillen X1 structure $CaBiO_2Cl$ and $SrBiO_2Cl$ (13). This paper deals with the crystal structure determination of the new compound $Bi_9V_2ClO_{18}$. The complete solid solution of the oxychloride vanadate and the oxychloride phosphate was also prepared. Its electrical properties and infrared study are reported in this paper.

0022-4596/98 $25.00

EXPERIMENTAL

Sample Preparation

Single crystals of $Bi_9V_2ClO_{18}$ were prepared as follows. Bi_2O_3, vanadium metal, and $KClO_3$ were mixed in a 1:3:2 molar ratio. About 1 g of the mixture was placed in a gold capsule and sealed in an evacuated silica tube. The tube was then heated at 600°C for 12 hr, after which the temperature was raised to 900°C and maintained for 24 hr. After cooling to room temperature (5°C/hr, fast), the crystalline product was slightly crushed and washed with water in an ultrasonic cleaner. Orange single crystals were isolated from the greenish unidentified powder matrix.

Polycrystalline samples with composition $Bi_9(V_{1-x}P_x)_2ClO_{18}$ were obtained by solid-state reaction between Bi_2O_3 (Aldrich), V_2O_5 (Aldrich), $(NH_4)_2HPO_4$ (Fluka), and BiOCl (Aldrich). Amounts of the starting materials were mixed in five $4:1-x:2x:1$ ($x = 0$, 0.25, 0.5, 0.75, and 1) molar ratios and thoroughly ground in an agate mortar. The mixtures were fired in alumina crucibles at 650°C for 3 days with an intermediate regrinding. The single-phase products of the reaction were examined by X-ray powder diffraction using a Guinier–Dewolff focusing camera and Cu$K\alpha$ radiation. No impurities were detected. The unit cell parameters were refined by least squares from $K\alpha_2$-corrected X-ray patterns using a Siemens D5000 powder diffractometer (Cu$K\alpha$ radiation) equipped with a back monochromator.

Crystal Structure Analysis

Weissenberg photographs with **b** as the rotating axis revealed a monoclinic unit cell with $a = 11.66$ Å, $b = 5.45$ Å, $c = 14.68$ Å, and $\beta = 93.7°$. No systematic extinction was detected on photographed layers.

X-ray single-crystal diffraction data were collected on a Philips PW1100 diffractometer with graphite-monochromatized Mo$K\alpha$ radiation. The data collection parameters are reported in Table 1. The reflections were corrected for background and Lorentz–polarization effects. The absorption corrections were performed using the analytical method of De Meulenaer and Tompa (14). The systematic absences in the reduced data ($0k0$, $k = 2n + 1$) indicated possible space groups $P2_1$ or $P2_1/m$. The structure determination was carried out satisfactorily in the centrosymmetric $P2_1/m$ space group. Direct methods (SHELXS-86 (15)) were used to locate bismuth atoms in eight 2(*e*) special positions. After refinement of their atomic coordinates and isotropic thermal parameters ($R = 0.228$, $R_w = 0.254$), a supplementary bismuth atom was found from Fourier difference maps to be disordered over two mirror-symmetry-related positions on a 4(*f*) site. Introduction in the refinement process of this atom (half-filled site) led to a significant convergence ($R = 0.132$, $R_w = 0.153$) and allowed location of the remaining atoms from subsequent F_O–F_{Bi} difference Fourier synthesis maps. It is noteworthy that O(11), O(12), and O(13) half-occupy general 4(*f*) positions. The final cycles of the full-matrix refinement included anisotropic temperature factors for Bi, V, and Cl and yielded $R = 0.035$ and $R_w = 0.041$. Neutral-atom scattering factors were obtained from the "International Tables for X-ray Crystallography" (16) and anomalous corrections were made according to Cromer and Liberman (17). The refinement was performed using a local modification of the SFLS-5 program (18). Reduction of the symmetry was considered, but that led to nonconvergent refinements with unacceptable thermal parameters and did not resolve the disorder problems. The atomic coordinates with isotropic and anisotropic thermal parameters are listed in Tables 2 and 3.

TABLE 1
Crystal Data, Intensity Measurement, and Structure Refinement Parameters for Single-Crystalline $Bi_9V_2ClO_{18}$

Crystal data	
Crystal symmetry	Monoclinic
Space group	$a = 11.671(2)$ Å, $b = 5.463(1)$ Å
Cell dimensions	$c = 14.792(3)$ Å, $\beta = 93.67(1)°$
	941.18
Volume (Å^3)	2
Data collection	
Equipment	Philips PW1100
λ(Mo$K\alpha$ (graphite monochromator))	0.7107 Å
Scan mode	ω–2θ
Scan width (deg)	1.3
θ range (deg)	2–30
Standard reflections	$2\bar{4}0$, $0\bar{4}\bar{2}$, $\bar{3}\bar{3}0$
measured every 2 hr (no decay)	
Recording reciprocal space	$-16 \le h \le 16$, $-7 \le k \le 7$,
	$0 \le l \le 20$
Number of measured reflections	5706
Number of reflections $I > 3\sigma(I)$	4105
Number of independent reflections	2270
μ (cm^{-1}) (for $\lambda(K\alpha) = 0.7107$ Å)	813.25
Limiting faces and distances (cm)	100
from an arbitrary origin	$\bar{1}00$, 0.031
	010
	$0\bar{1}0$, 0.136
	001
	$00\bar{1}$, 0.020
	101
	$\bar{1}0\bar{1}$, 0.031
	$\bar{1}01$, 0.020
Transmission factor range	0.02–0.08
Merging R factor	0.034
Refinement	
Number of refined parameters	124
$R = \sum[\lvert F_o\rvert - \lvert F_c\rvert]/\sum\lvert F_o\rvert$	0.035
$R_w = [\sum_w(\lvert F_o\rvert - \lvert F_c\rvert)^2/\sum wF_o^2]^{1/2}$	0.041
with $w = 1/\sigma(F_o)$	

TABLE 2
Positional and Isotropic or Equivalent Thermal Parameters for $Bi_9V_2ClO_{18}$

Atom	Site and occupancy	x	y	z	B_{iso} or B_{eq} (Å^2)
Bi(1)	2(*e*), 1	0.30514(6)	$\frac{1}{4}$	0.21706(5)	0.71(2)
Bi(2)	2(*e*), 1	0.54312(6)	$\frac{1}{4}$	0.65271(5)	0.64(2)
Bi(3)	2(*e*), 1	0.86075(6)	$\frac{1}{4}$	0.66356(5)	0.96(2)
Bi(4)	2(*e*), 1	0.95414(6)	$\frac{1}{4}$	0.15650(5)	0.97(2)
Bi(5)	2(*e*), 1	0.61437(6)	$\frac{1}{4}$	0.20042(6)	1.11(2)
Bi(6)	2(*e*), 1	0.26125(6)	$\frac{1}{4}$	0.47071(5)	0.84(2)
Bi(7)	2(*e*), 1	0.26166(6)	$\frac{1}{4}$	0.95538(5)	0.68(2)
Bi(8)	2(*e*), 1	0.96168(6)	$\frac{1}{4}$	0.41215(5)	0.76(2)
Bi(9)	4(*f*), $\frac{1}{2}$	0.55723(8)	0.3057(2)	0.91299(8)	1.23(3)
V(1)	2(*e*), 1	0.1984(2)	$\frac{1}{4}$	0.7196(2)	0.57(7)
V(2)	2(*e*), 1	0.8609(3)	$\frac{1}{4}$	0.9070(3)	1.13(9)
Cl	2(*e*), 1	0.5715(8)	$\frac{1}{4}$	0.4330(5)	3.4(2)
O(1)	4(*f*), 1	0.5995(8)	− 0.003(2)	0.0861(7)	1.1(2)
O(2)	4(*f*), 1	0.4538(7)	− 0.001(2)	0.2279(7)	0.6(1)
O(3)	4(*f*), 1	0.2950(8)	0.505(2)	0.3599(7)	1.0(2)
O(4)	4(*f*), 1	0.1047(8)	0.493(2)	0.4526(7)	0.8(2)
O(5)	2(*e*), 1	0.3613(15)	$\frac{1}{4}$	0.0768(14)	2.0(3)
O(6)	2(*e*), 1	0.7612(16)	$\frac{1}{4}$	0.8196(15)	2.3(4)
O(7)	4(*f*), 1	0.1872(10)	0.004(3)	0.2101(9)	2.0(2)
O(8)	2(*e*), 1	0.0466(15)	$\frac{1}{4}$	0.2814(13)	2.0(3)
O(9)	2(*e*), 1	0.0975(17)	$\frac{1}{4}$	0.6333(15)	2.5(4)
O(10)	2(*e*), 1	0.3311(16)	$\frac{1}{4}$	0.6865(15)	2.2(4)
O(11)	4(*f*), $\frac{1}{2}$	0.9880(18)	0.151(5)	0.8818(16)	1.4(4)
O(12)	4(*f*), $\frac{1}{2}$	0.8725(18)	0.586(5)	0.9136(16)	1.5(4)
O(13)	4(*f*), $\frac{1}{2}$	0.8109(20)	0.165(5)	1.0025(17)	2.0(4)

TABLE 3
Anisotropic Displacement Parameters for Bismuth, Vanadium, and Chlorine Atoms of $Bi_9V_2ClO_{18}$[a]

Atom	U_{11}	U_{22}	U_{33}	U_{12}	U_{13}	U_{23}
Bi(1)	0.0061(3)	0.0112(4)	0.0096(4)	0	0.0004(2)	0
Bi(2)	0.0085(3)	0.0092(4)	0.0064(3)	0	− 0.0010(2)	0
Bi(3)	0.0080(3)	0.0216(5)	0.0067(3)	0	0.0010(2)	0
Bi(4)	0.0064(3)	0.0238(5)	0.0068(3)	0	0.0004(2)	0
Bi(5)	0.0074(3)	0.0250(5)	0.0096(4)	0	0.0005(3)	0
Bi(6)	0.0102(3)	0.0163(4)	0.0055(3)	0	− 0.0006(2)	0
Bi(7)	0.0075(3)	0.0114(4)	0.0069(3)	0	0.0001(2)	0
Bi(8)	0.0078(3)	0.0112(4)	0.0099(4)	0	0.0005(2)	0
Bi(9)	0.0095(4)	0.0158(9)	0.0221(5)	0.0044(4)	0.0041(4)	0.0083(5)
V(1)	0.006(1)	0.008(2)	0.008(2)	0	− 0.001(1)	0
V(2)	0.006(1)	0.032(2)	0.006(1)	0	0.000(1)	0
Cl	0.081(6)	0.026(4)	0.022(4)	0	0.0004(4)	0

[a] The anisotropic temperature factors are defined by

$$U = \exp[-2\pi^2(U_{11}h^2a^{*2} + \ldots + 2U_{23}klb^*c^*)].$$

Table 4 provides selected bond distances and angles in $Bi_9V_2ClO_8$.

Powder X-ray diffraction data for $Bi_9V_2ClO_{18}$, prepared as described in the experimental section, were indexed using the monoclinic unit cell parameters determined from the single-crystal experiment. Indicies were assigned on the basis of Lazy Pulverix (19) simulation of the structure after least-squares minimization of the parameters. Observed and calculated Bragg angles intensities are reported in Table 5 for a 2θ limit equal to 40°.

Characterization

Infrared data were recorded using a Perkin-Elmer 1730 Fourier transform spectrophotometer in the 1500 to 400 cm^{-1} region. Samples corresponding to $x = 0, 0.25, 0.5, 0.75$, and 1 were pelleted in a KBr matrix. For each composition, the air spectrum was subtracted from the obtained data.

Investigations of the electrical properties were carried out on sintered materials. Cylindrical pellets (diameter 6 mm, $\approx$5 mm thick) were obtained using a conventional cold press and were sintered at 650°C for 12 hr in gold foil boats. Gold electrodes were vacuum deposited on both flat surfaces of the samples. Conductivity measurements were carried out by ac impedance spectroscopy over the range 1–10^6 Hz with a Solartron 1170 frequency-response analyzer and an HP-85 calculator. Measurements were made at 15°C intervals over the 300–600°C range on both heating and cooling after a first temperature cycle. Each set of values were recorded at a given temperature after a 1-hr stabilization time.

DESCRIPTION OF THE STRUCTURE AND DISCUSSION

The projection of the structure on the (010) plane (Fig. 1) shows that the tridimensional framework is built up from corner- and edge-sharing BiO_3 or BiO_4 pyramids and single VO_4 tetrahedra. This framework creates tunnels with an elliptical cross section running along **b** and occupied by Cl^- anions.

As observed in many compounds containing cations with a lone pair of electrons, the bismuth coordinations are complex and irregular. Both short and long bond lengths are observed: The bismuth atoms typically coordinate more tightly with three or four atoms on one side (bond lengths 2.10–2.40 Å) and less tightly with three, four, or five atoms on the other side (bond lengths 2.40–2.90 Å). These two bunches of neighbors clearly involve the $6s^2$ lone pair steric effect and correspond to the two distinct Bi–O length ranges, 2.08–2.29 Å and 2.48–2.80 Å, observed in α-Bi_2O_3 (20). In $Bi_9V_2ClO_{18}$, if only the short distances on one side are considered, Bi(1), Bi(4), Bi(7), and Bi(8) are surrounded by three oxygen atoms, forming with the bismuth atom trigonal pyramids whereas Bi(2), Bi(3), Bi(5), Bi(6), and Bi(9) are surrounded by four oxygens, leading to BiO_4 square

TABLE 4
Interatomic Distances of Bi, V, and Cl Atoms for $Bi_9V_2ClO_{18}$, Angles for the Vanadium Atom Environments, and s_{ij} Calculations

Bi(1) environment	d (Å)	s_{ij}	$\sum s_{ij}$	Bi(2) environment	d (Å)	s_{ij}	$\sum s_{ij}$
Bi(1)–O(2)	2.210(9)	0.7309		Bi(2)–$O(2)^{ii}_{101}$	2.227(11)	0.6981	
–$O(2)^{iv}$				–$O(2)^{iii}_{101}$			
–O(3)	2.541(11)	0.2988		–$O(3)^{iii}_{111}$	2.333(10)	0.5242	
–$O(3)^{iv}$				–$O(3)^{ii}_{111}$			
–O(5)	2.216(21)	0.7191		–O(11)	2.555(19)	0.2877	
–$O(6)^{ii}_{101}$	2.882(6)	0.1189		–Cl	3.288(8)	0.0994	
–$O(6)^{ii}_{111}$				–Cl^{ii}_{101}	3.262(5)	0.1067	
–$O(13)^{ii}_{111}$	2.886(22)	0.1176	3.13	–Cl^{ii}_{111}		0.1067	3.04
Bi(3) environment	**d (Å)**	**s_{ij}**	**$\sum s_{ij}$**	**Bi(4) environment**	**d (Å)**	**s_{ij}**	**$\sum s_{ij}$**
Bi(3)–$O(3)^{ii}_{111}$	2.266(10)	0.6282		Bi(4)–$O(7)^{ii}_{101}$	2.312(14)	0.5548	
–$O(3)^{iii}_{111}$				–$O(7)^{iii}_{101}$			
–$O(4)^{ii}_{111}$	2.274(11)	0.6148		–$O(8)_{100}$	2.079(18)	1.0414	
–$O(4)^{iii}_{111}$				–$O(11)^{ii}_{201}$	2.372(27)	0.4717	
–O(5)	2.650(22)	0.2225		–$O(12)^{ii}_{211}$	2.498	0.3356	
–$O(9)_{100}$	2.827(20)	0.1379	2.85	–$O(13)_{001}$	2.777	0.1579	3.12
Bi(5) environment	**d (Å)**	**s_{ij}**	**$\sum s_{ij}$**	**Bi(6) environment**	**d (Å)**	**s_{ij}**	**$\sum s_{ij}$**
Bi(5)–O(1)	2.182(11)	0.7883		Bi(6)–O(3)	2.206(11)	0.7388	
–$O(1)^{iv}$				–$O(3)^{iv}$			
–O(2)	2.379(9)	0.4629		–O(4)	2.261(10)	0.6368	
–$O(2)^{iv}$				–$O(4)^{iv}$			
–$O(7)^{ii}_{101}$	2.668(13)	0.2200		–Cl	3.699(9)	0.0327	
–$O(7)^{iii}_{101}$				–Cl^{ii}_{101}	3.598(6)	0.0430	
–Cl	3.508(8)	0.0549	2.99	–Cl^{ii}_{111}	3.598(6)	0.0430	2.87
Bi(7) environment	**d (Å)**	**s_{ij}**	**$\sum s_{ij}$**	**Bi(8) environment**	**d (Å)**	**s_{ij}**	**$\sum s_{ij}$**
Bi(7)–$O(1)^{ii}_{101}$	2.225(10)	0.7018		Bi(8)–$O(4)_{100}$	2.187(10)	0.7777	
–$O(1)^{iii}_{101}$				–$O(4)^{iv}_{100}$			
–$O(5)_{001}$	2.076(19)	1.0499		–$O(4)^{ii}_{111}$	2.602(11)	0.2534	
–$O(13)^{ii}_{102}$	2.513(27)	0.3222		–$O(4)^{iii}_{111}$			
–$O(12)^{ii}_{112}$	2.720(24)	0.1842		–$O(8)_{100}$	2.229(19)	0.6943	
–O(7)	2.897(14)	0.1141		–$O(9)^{ii}_{101}$	2.886(7)	0.1176	
–$O(7)^{iv}$			3.19	–$O(9)^{ii}_{111}$	3.598(6)		2.99
Bi(9) environment	**d (Å)**	**s_{ij}**	**$\sum s_{ij}$**	**Cl environment**	**d (Å)**	**s_{ij}**	**$\sum s_{ij}$**
Bi(9)–$O(1)^{ii}_{101}$	2.467(10)	0.3649		Cl–Bi(2)	3.288(8)	0.0994	
–$O(1)^{iii}_{101}$	2.107(10)	0.9655		–$Bi(2)^{ii}_{101}$	3.262(5)	0.1067	
–$O(2)^{ii}_{101}$	2.663(11)	0.2148		–$Bi(2)^{ii}_{111}$		0.1067	
–$O(2)^{iii}_{101}$	2.332(11)	0.5256		–Bi(5)	3.508(8)	0.0549	
–$O(5)^{ii}_{111}$	2.608(6)	0.2493		–Bi(6)	3.699(9)	0.0327	
–$O(6)^{iv}_{001}$	2.793(10)	0.1512		–$Bi(6)^{ii}_{101}$	3.598(6)	0.0430	
–O(6)	2.844(20)	0.1317	2.60	–$Bi(6)^{ii}_{111}$		0.0430	0.48
V(1) environment	**d (Å)**	**s_{ij}**	**$\sum s_{ij}$**	**V(2) environment**	**d (Å)**	**s_{ij}**	**$\sum s_{ij}$**
V(1)–O(7)	1.743(15)	1.176		V(2)–O(6)	1.683(20)	1.383	
–$O(7)^{iv}$	1.743(15)	1.176		–O(11)	1.644(23)	1.537	
–O(9)	1.680(21)	1.394		–O(12)	1.843(27)	0.897	
–O(10)	1.654(19)	1.496	5.24	–O(13)	1.630(26)	1.596	5.41

Angles (deg)[a]		Angles (deg)[a]	
O(7)–V(1)–$O(7)^{iv}$	105.5	O(6)–V(2)–O(11)	114.5
O(7)–V(1)–O(9)	112.3	O(6)–V(2)–O(12)	94.9
$O(7)^{iv}$–V(1)–O(9)	112.3	O(6)–V(2)–O(3)	113.4
O(7)–V(1)–O(10)	106.3	O(11)–V(2)–O(12)	106.0
$O(7)^{iv}$–V(1)–O(10)	106.3	O(11)–V(2)–O(13)	118.7
O(9)–V(1)–O(10)	106.3	O(12)–V(2)–O(13)	105.5

[a] The standard deviations of the angles are approximately 2°.

pyramids (Fig. 2). The oxygen and chlorine atoms complete the coordination of bismuth atoms to obtain $Bi(1,7,8,9)O_7$, $Bi(2)O_5Cl_3$, $Bi(3,4)O_6$, $Bi(5)O_6Cl$, and $Bi(6)O_4Cl_3$. Thus bismuth atoms are 6–7–8 coordinated, with Bi–O and Bi–Cl distances ranging from 2.076(19) to 2.897(14) Å and from 3.262(5) to 3.699(9) Å, respectively. The VO_4/PO_4 tetrahedra are isolated, which is typical of orthovanadate–phosphate compounds.

The O(1), O(2), O(3), and O(4) atoms are nearly coplanar and form edge-sharing O_4 squares similar to those existing in $[Bi_2O_2]^{2+}$ layers of the Aurivillius phases. The Bi(1), Bi(2), Bi(3), Bi(5), Bi(6), and Bi(9) atoms are alternately above and below the oxygen planes, approximately at the apex of the center of the O_4 squares, yielding edge-sharing $Bi(n)O_4$ ($n = 1, 2, 3, 5, 6, 9$) square pyramids (Fig. 3). However, Bi(1) is far from O(3) and the nearest O(5) atoms so its polyhedron is better described as a BiO_3 pyramid. A $Bi(1)O_3$ trigonal pyramid shares an O(2)–O(2) edge with a $Bi(5)O_4$ square pyramid whereas $Bi(7)O_3$ and $Bi(8)O_3$ edge-share $Bi(9)O_4$ and $Bi(6)O_4$, respectively. $Bi(4)O_3$ and $Bi(8)O_3$ are connected by the O(8) corner. This leads to the basal bismuth–oxygen unit $(Bi_9O_{13})_\infty$. Two such units related by a twofold helicoidal axis are connected by O(5) oxygen atoms. Thus two sheets of square pyramids of formula $Bi(2)Bi(3)Bi(5)Bi(6)Bi(9)O_8$ are connected by two $Bi(1)Bi(7)O_5$ corner-sharing pyramids and are terminated at each extremity by one $Bi(8)Bi(4)O_5$ corner-sharing pyramid. The formula of the unit obtained is $Bi_{18}O_{24}$, shown in Fig. 3. Finally, the $V(1)O_4$ tetrahedron bridges two consecutive (along **b**) $Bi(4)O_3$ trigonal pyramids via O(7) corners and, so, sits at the periphery of the large tunnels. The complex $[Bi_{18}V(1)_2O_{28}]_\infty$ units and the $V(2)O_4$ are connected to each other via weak Bi–O bonds. In Fig. 1, Bi–O bonds with distances shorter than 2.7 Å are represented with solid lines whereas longer bonds are drawn as dotted lines. In the $V(1)O_4$ tetrahedron, two distinct V–O distance groups are observed; the distances with O(9) and O(10) atoms, not involved in a strong Bi–O bond, are shorter than

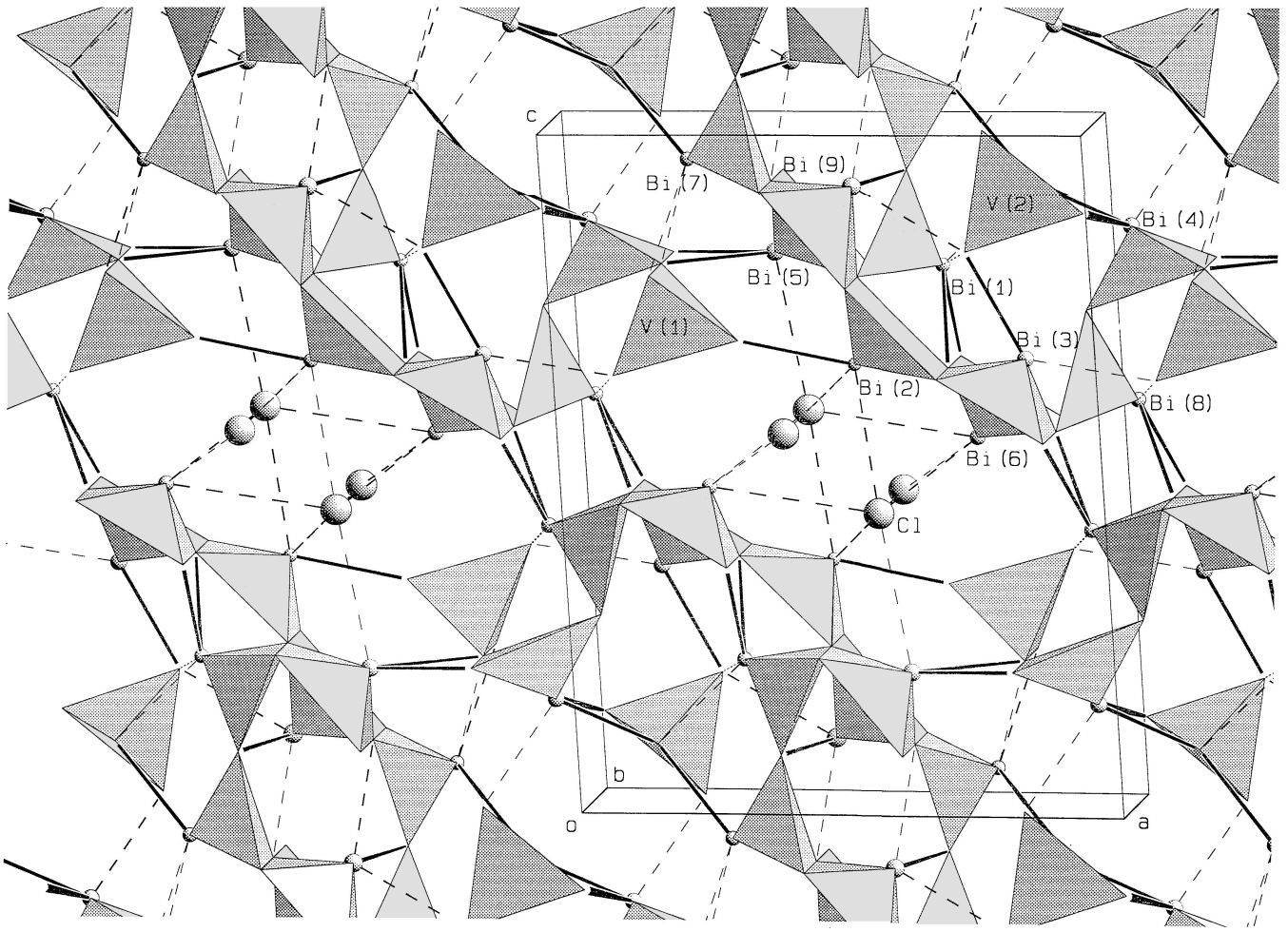

FIG. 1. Projection of the $Bi_9V_2ClO_{18}$ crystal structure on the (010) plane.

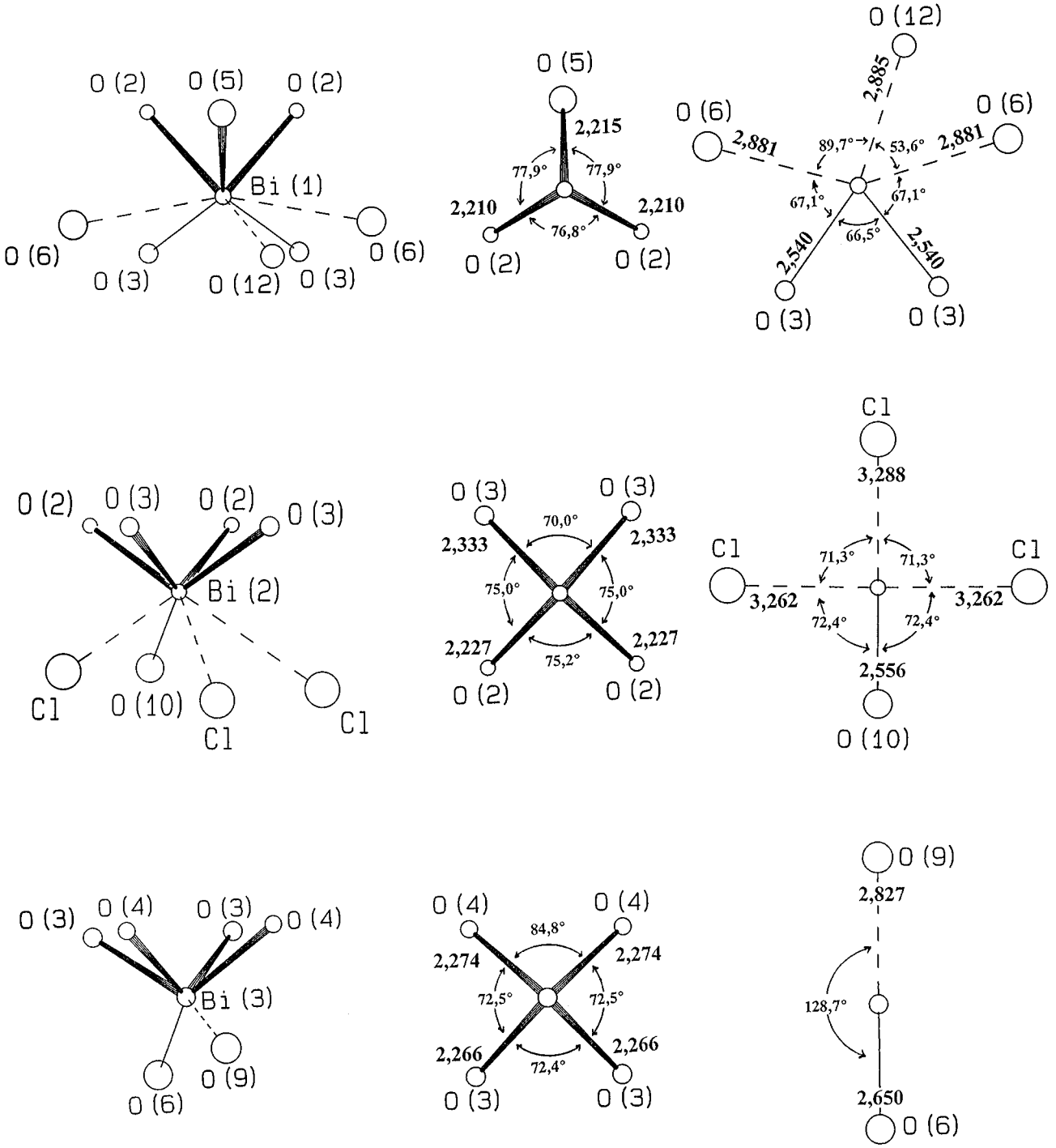

FIG. 2. Bi^{3+} environment from Bi(1) to Bi(9).

the distances with O(7) atoms shared with a bismuth trigonal pyramid. The $V(2)O_4$ tetrahedron occupies two symmetrically related positions: the O(6) atom in the *m* mirror is common to the two positions whereas O(11), O(12), and O(13) are half-occupied; astonishingly, the V(2)–O(12) distance is significantly longer than the three other V(2)–O distances. However, the average V–O distance found for both V(1) and V(2) tetrahedra is 1.70 Å.

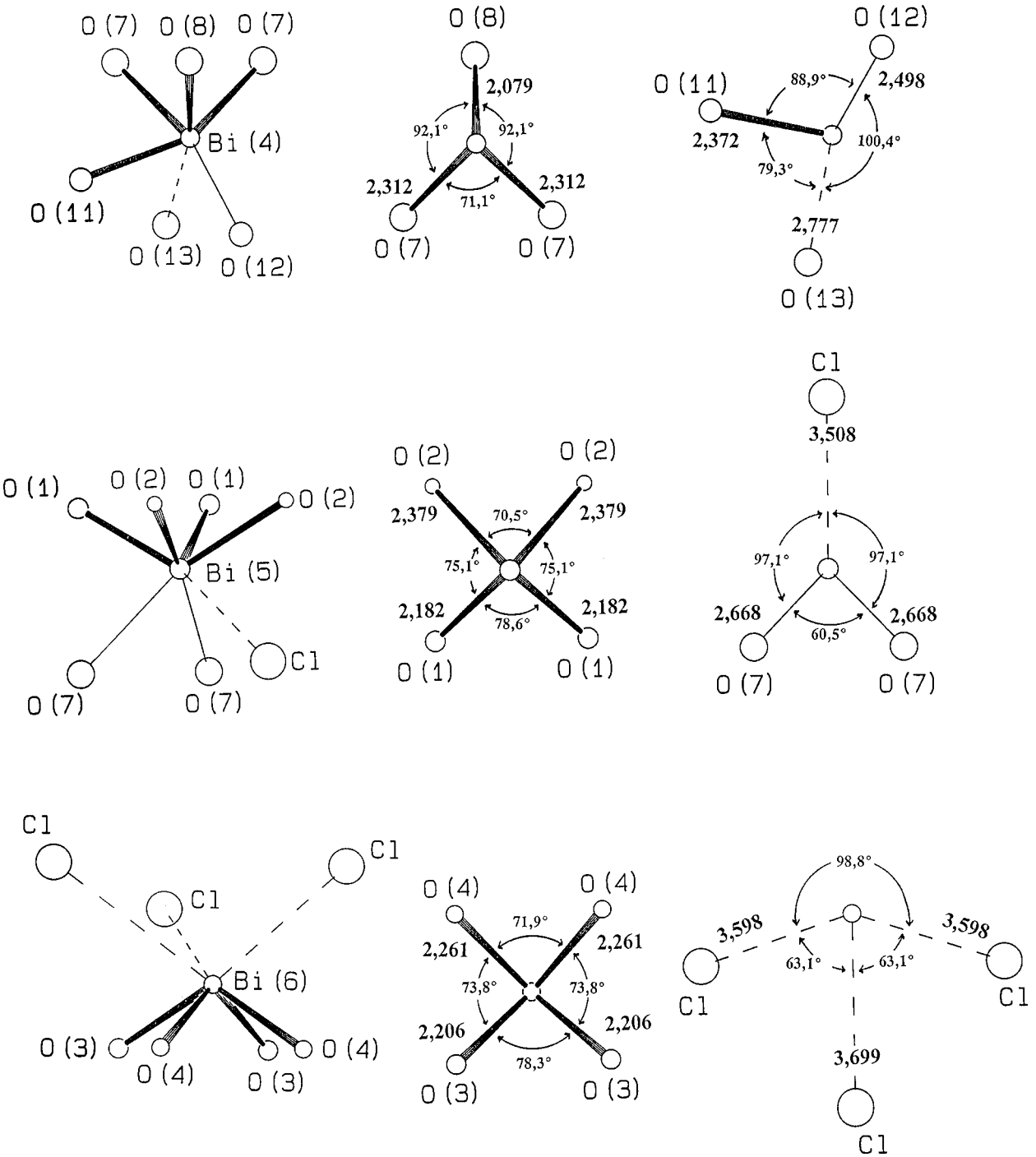

FIG. 2—*Continued*

Bond Valences

The sums of the electrostatic valences were calculated with the Brown and Altermatt data (21) for Bi–O (r_0 = 2.094 Å, $B = 0.37$) and with value of r_0 calculated from Bi–Cl distances in bismuth trichloride (22) (r_0 = 2.434 Å, $B = 0.37$). Results for the complete coordination of the cations are listed in Table 4. The valences calculated for the independent bismuth atoms, which range from 2.85 to 3.19, are in good agreement with the formal charge +3 of this

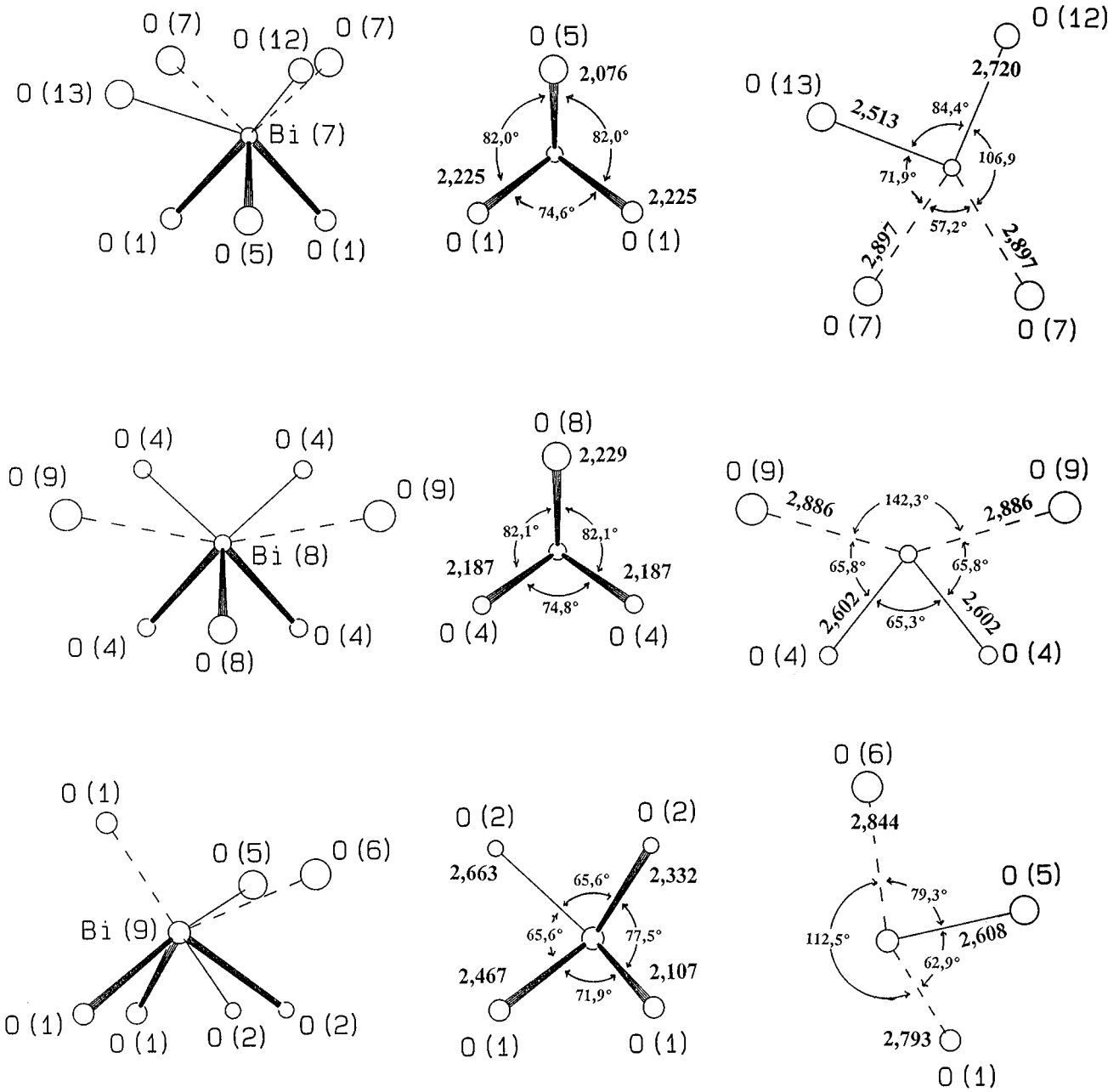

FIG. 2—*Continued*

cation. However, Bi(9) seems underbonded (electrostatic valence sum = 2.60), related to its delocalization over two equivalent positions. The valence electrostatic sum calculated for V(2) is 5.41, higher than the expected value for V^{5+}. That certainly reflects the disorder over the $V(2)O_4$ tetrahedron. On the other hand, the 5.24 value calculated for V(1) matches better.

The chloride ions are located in the elliptical tunnels delimited by the Bi–V–O framework. Chlorides are weakly bonded to bismuth atoms, with Bi–Cl distances ranging from 3.262(5) to 3.699(9) Å; no short Bi–Cl distances are observed and the electrostatic valence sum calculation of 0.5 indicates an underbonded character. Nevertheless, short Bi–Cl distances are observed in several compounds as, for example, in bismuth trichloride, where bismuth is strongly bonded to three chloride ions at 2.468, 2.513, and 2.518 Å, forming a distorted trigonal pyramid. Five more Cl^- sit at distances between 3.216 and 3.450 Å on the opposite side. In

TABLE 5
Observed and Calculated X-Ray Powder Diffraction Patterns for $Bi_9V_2ClO_{18}$ from Siemens D5000 Goniometer Data (λ = 1.54056 Å)[a]

hkl	$2\theta_{obs}$ (deg)	$2\theta_{calc}$ (deg)	I_{obs}/I_0	I_{calc}/I_0
101	9.95	9.96	13	33.9
102	14.59	14.60	16	14.3
$11\bar{1}$	18.78	18.75	3	2.3
$20\bar{2}$	18.83	18.78	1	2.3
111	19.06	19.06	3	2.9
012	20.20	20.20	2	4.2
$11\bar{2}$	21.34	21.33	5	7.6
112	21.88	21.88	4	5.8
004	24.06	24.09	3	1.8
013	24.33	24.32	4	6.6
$11\bar{3}$	25.16	25.16	15	25.1
113	25.87	25.86	5	8.5
$20\bar{4}$	27.77	27.75	14	10.8
310	28.17	28.17	66	91.1
$31\bar{1}$	28.49	28.51	33	32.6
311	29.13	29.14	60	28.9
014	29.18	29.18	100	100
204	29.44	29.44	18	15.9
$11\bar{4}$	29.79	29.78	6	11.7
303	30.20	30.19	15	12.1
114	30.60	30.59	15	17
$30\bar{4}$	32.35	32.35	36	26.9
020	32.75	32.76	29	52.9
304	34.57	34.56	13	10.9
$40\bar{3}$	34.75	34.75	9	6.7
410	34.87	34.88	13	7.1
403	36.83	36.83	5	3.7
$30\bar{5}$	37.01	37.02	7	3.9
412	37.67	37.68	5	4.8
305	39.50	39.47	3	3.0
413	40.45	40.47	3	2.4

[a]Refined parameters: $a = 11.671(2)$ Å, $b = 5.463(1)$ Å, $c = 14.792(3)$ Å, and $\beta = 93.67(1)^\circ$

TABLE 6
Bismuth Oxychloro Polyhedron for Various Compounds

Compound	Bi–O (Å)	Bi–Cl (Å)
Bi_4NbO_8Cl (24)[a]		
Bi(2)	2.19–2.32 (×4)	3.16–3.51 (×4)
Bi(4)	2.04–2.43 (×4)	3.16–3.46 (×4)
$PbBi_3WO_8Cl$ (24)		
Bi(3)	2.29 (×4)	3.40 (×4)
Bi(4)	2.24 (×4)	3.31 (×4)
$LaBi_2O_4Cl$ (25)	2.25 (×4)	3.39 (×4)
$SrBiO_2Cl$ (13)	2.21 (×4)	3.49–3.52 (×4)
$CaBiO_2Cl$ (13)	2.06–2.26 (×4)	3.43–3.47 (×3)
$BiSr_3O_3Cl_3$ (26)	2.06–2.07 (×3)	3.47 (×2)
BiOCl (23)	2.31 (×4)	3.07–3.49 (×5)
$Bi_9V_2ClO_{18}$		
Bi(2)	2.22–2.33 (×4)	3.26–3.28 (×3)
Bi(6)	2.20–2.26 (×4)	3.59–3.69 (×3)

[a]Indicates the reference providing the data.

BiOCl, four oxygen atoms and four chloride ions form a distorted square antiprism similar to the polyhedron coordination of Bi(2) but the Bi–Cl are significantly shorter (3.07 Å) (23). Bismuth coordinated by oxygen atoms at short distances on one side and by chlorine atoms at long distances indicates the location of the lone pair of electrons toward the center of the chlorine polygon. They are observed in several compounds, e.g., in the Sillen phases and in the Bipox family crystal structure, which is a combination of Aurivillius and Sillen phases (24). Table 6 provides various examples of this kind of coordination for Bi^{3+}.

PO_4^{3-} Substitution for VO_4^{3-}

The phosphate-analogous compound $Bi_9P_2ClO_{18}$ and a continuous solid solution of formula $Bi_9(V_{1-x}P_x)_2ClO_{18}$

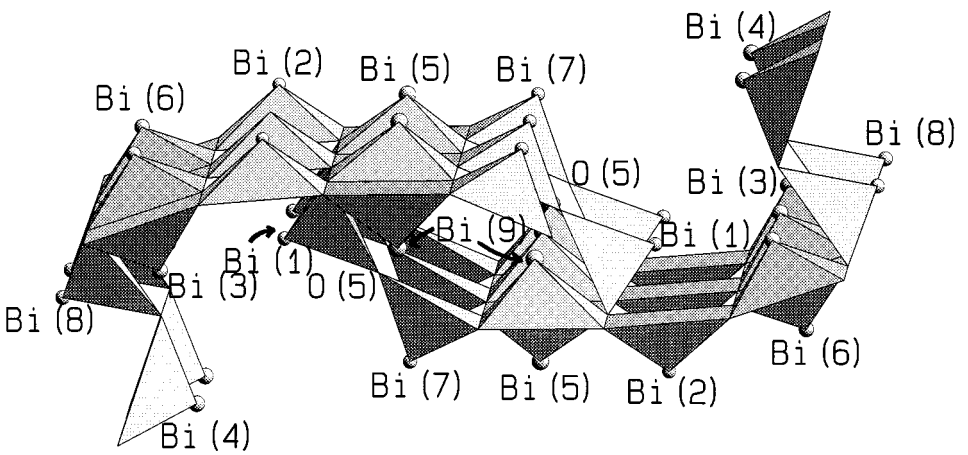

FIG. 3. Bismuth polyhedra linkage forming the $Bi_{18}O_{24}$ entity.

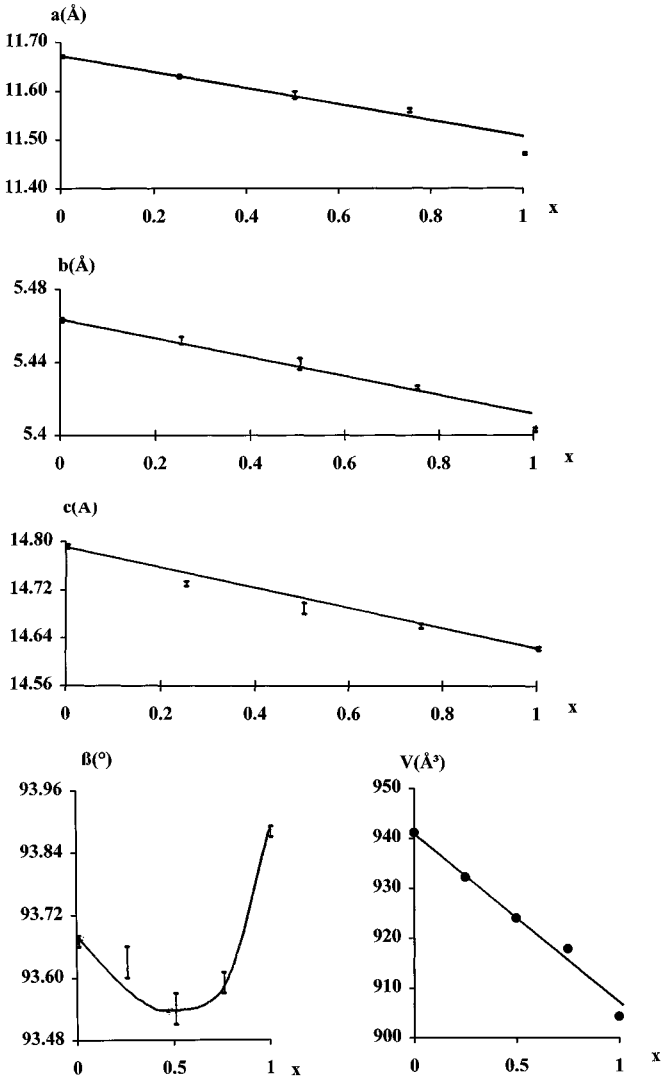

FIG. 4. Unit cell parameters versus x for $Bi_9(V_{1-x}P_x)_2ClO_{18}$.

were prepared. The refined unit cell parameters for $Bi_9P_2ClO_{18}$ and three compositions of the solid solution are reported in Fig. 4. a, b, and c linearly decrease upon substitution of V with P species whereas β passes through a minimum for $x = 0.5$. The linear evolution of the unit cell volume is in accordance with the lower ionic radius of P^{5+} (0.17 Å) as compared to V^{5+} (0.35 Å) in IV coordination from ref 27. Thus, the unit cell is assumed to shrink because of the consequent shortness of the P–O distances involved in the framework.

Infrared Study

A free PO_4^{3-}/VO_4^{3-} ion under T_d symmetry has four fundamental vibrations: the nondegenerate symmetric stretching mode ν_1 (A_1), the doubly degenerate symmetric bending mode ν_2 (E), the triply degenerate asymmetric stretching mode ν_3 (F_2), and the triply degenerate asymmetric bending mode ν_4 (F_2). To assign accurately the different bands of the IR spectra, we have to predict what these fundamental vibrations will become in our crystallized solids. Factor group analysis of the compounds was carried out using the correlation method developed by Fateley *et al.* (28). Our IR study was realized on the basis of works (29–33) on the vibrational spectroscopy of PO_4^{3-} molecules. The correlation was effected between the MO_4^{3-} free-ion symmetry (T_d), the site symmetry (C_s), and the factor group symmetry (C_{2h}). It is meaningful to notice that, because of the statistical disorder occurring around V(2), we must consider six V/P independent atoms per reduced unit cell. Thus, since $g(C_{2h})/g(C_s)$ equals 2, the results of the factor group must be multiplied by 2. Since only *ungerade* orientations are IR active in the C_{2h} factor group symmetry, we expect the following components for

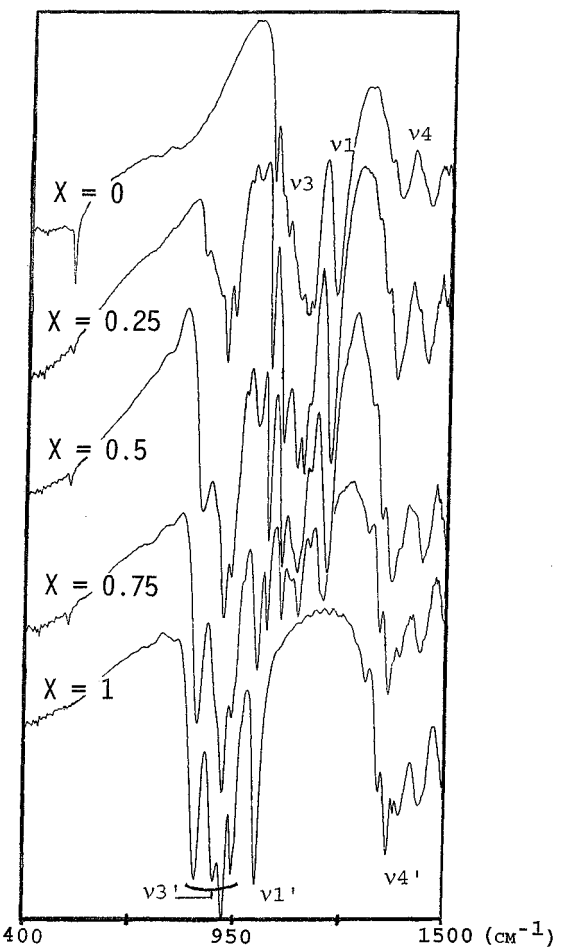

FIG. 5. Infrared spectra for $Bi_9(V_{1-x}P_x)_2ClO_{18}$.

each mode:

stretching: $\nu_1(s)$, $3B_u$; ν_3(as), 6Bu + $3A_u$

bending: ν_2(s), $3B_u + 2A_u$; ν_4(as), $6B_u + 2A_u$

$Bi_9V_2ClO_{18}$: As shown in Fig. 5, in the explored domain, only the ν_1, ν_3, and ν_4 modes are observed.

The ν_3 mode of PO_4^{3-} appears, with degeneracy lifted, between 761 and 865 cm^{-1}. It is composed of five distinct peaks (761, 774, 794, 831, and 865 cm^{-1}) and two shoulders (800 and 840 cm^{-1}). This is in good agreement with the predicted nine-band split of this massif.

The ν_4 mode appears from 400 to 560 cm^{-1} and is expected to continue below 400 cm^{-1}. From the complex shape of its massif (nine components are predicted), two

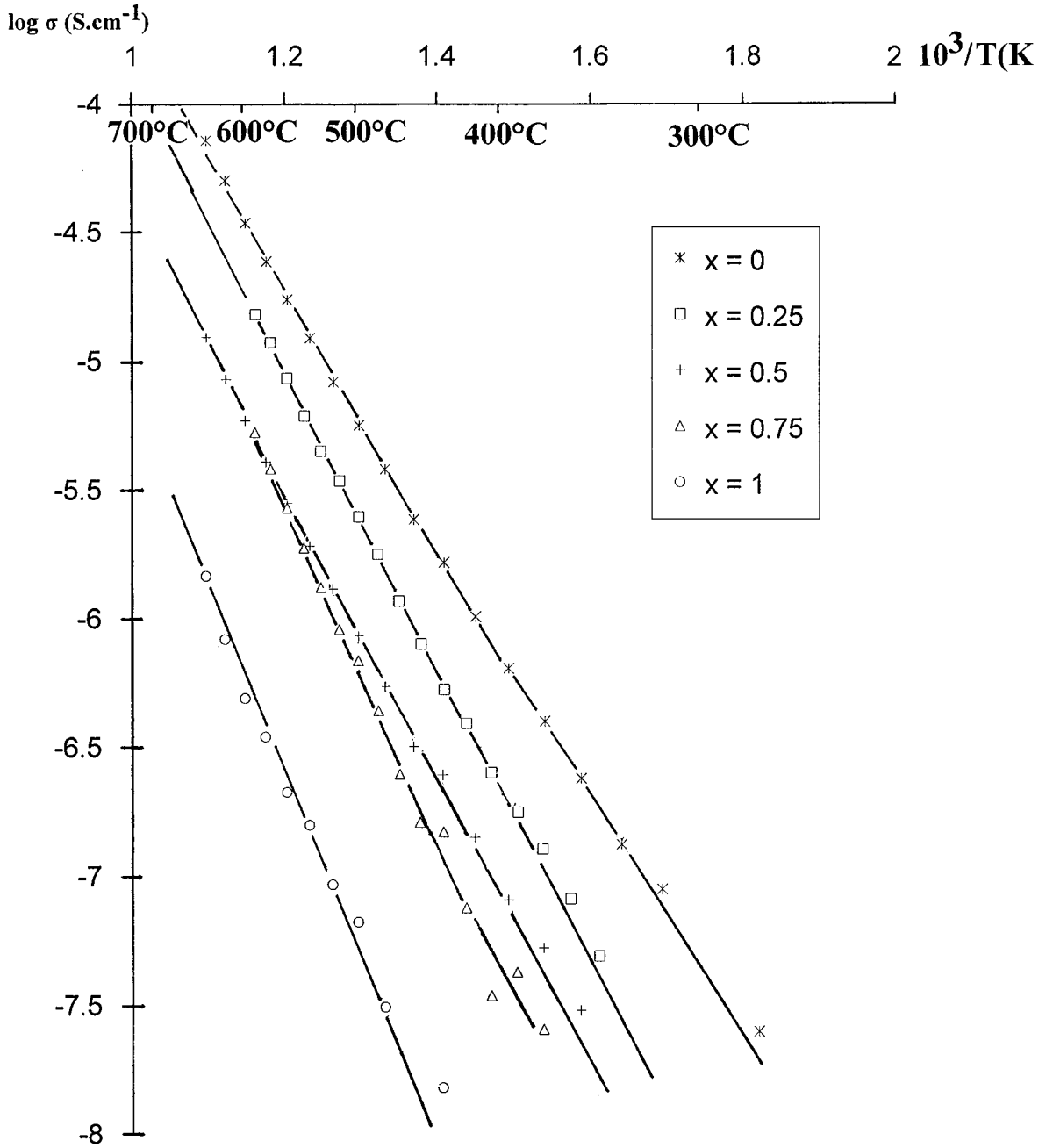

FIG. 6. log(σ) thermal evolution (vs 1000/T) for the solid solution.

stronger peaks are observed at respectively 453 and 533 cm^{-1}.

The three B_u orientations predicted for the ν_1 mode appear at the same 700-cm^{-1} wavenumber as a strong characteristic band.

The intermediate compounds show a progressive vanishing of the VO_4^{3-} bands, yielding a growth of the PO_4^{3-} vibrations. In $Bi_9P_2ClO_{18}$, ν_3 consists of four large bands at 955, 978, 1004, and 1051 cm^{-1} whereas ν_1 is observed as a single band at 894 cm^{-1}. This strong shift of the stretching vibration modes toward higher wavenumbers from the V to the P compounds clearly indicates that the P–O bonds are stronger than the V–O bonds already discussed. At the same time, there is no drastic change in the ν_4 bending mode position, which still appears as a very complex multiplet. This vibration mode, only involving angular displacement, is not assumed to sustain a V^{5+}/P^{5+} contrast.

Electrical Properties

As previously described, the crystal structure of $Bi_9V_2ClO_{18}$ reveals a weakly bonded character of the chloride anions in the one-dimensional tunnels whereas oxide anions are, at a minimum, strongly bonded to one cation and to many more in most of the cases. This consideration suggests a certain mobility of the Cl^- species, although without other selective experiments such as transport number measurements, O^{2-} contribution to the conductivity cannot be ruled out. Thus, conductivity was measured in air for the complete series $Bi_9(V_{1-x}P_x)_2ClO_{18}$ $(0 \le x \le 1)$ by the complex impedance method. Figure 6 gives the temperature-dependent ionic conductivity for $x = 0$, 0.25, 0.5, 0.75, and 1 collected upon the second heating. A linear Arrhenius type law is seen for all investigated samples over the entire temperature range studied. The conductivity values remain low; however, the conductivity reaches $10^{-4}\,\Omega^{-1}\,cm^{-1}$ for the vanadium compound at 650°C, an interesting value if a chloride-only mobility is considered. It is somewhat far to compete with the attractive results of some alkaline earth halides such as $BaCl_2$ above its displacive transition (34). In our compounds the conductivity decreases whereas the activation energy slightly increases during the substitution from $Bi_9V_2ClO_8$ ($E_a = 0.93$ eV) to $Bi_9P_2ClO_{18}$ ($E_a = 1.22$ eV). This is in good agreement with the decrease of the tunnel cross section related to the *a* and *c* parameters. Several bismuth and chloride substitutions are planned to improve the electrical conductivity results.

REFERENCES

1. F. Abraham, M. F. Debreuille-Gresse, G. Mairesse, and G. Nowogrocki, *Solid State Ionics* **28–30,** 529 (1988).
2. F. Abraham, J. C. Boivin, G. Mairesse, and G. Nowogrocki, *Solid State Ionics* **40–41,** 934 (1990).
3. O. Joubert, A. Jouanneaux, and M. Ganne, *Mater. Res. Bull.* **29**, 175 (1994).
4. G. Mairesse, *in* "Fast Ion Transport in Solids" (B. Scorsati, Ed.), p. 271. Kluwer, Dordrecht, 1993.
5. O. Joubert, A. Jouanneaux, and M. Ganne, *Nucl. Instrum. Methods Phys. Res. Sect. B* **97,** 119 (1995).
6. J. Galy, R. Enjalbert, P. Millan, and A. Castro, *C. R. Acad. Sci., Ser. II* **317,** 43 (1993).
7. A. Ramanan, J. Gopalakrishan, and C. N. R. Rao, *J. Solid State Chem.* **60,** 376 (1985).
8. F. Abraham and O. Mentre, *J. Solid State Chem.* **109,** 127 (1994).
9. F. Abraham, J. Trehoux, and D. Thomas, *Mater. Res. Bull.* **13,** 805 (1978).
10. F. Abraham, J. Trehoux, and D. Thomas, *Mater. Res. Bull.* **12,** 43 (1978).
11. F. Abraham, J. Trehoux, and D. Thomas, *J. Solid State Chem.* **32,** 151 (1980).
12. H. Kämmerer and R. C. Gruehn, *J. Solid State Chem.* **112,** 81 (1996).
13. S. M. Fray, C. J. Milne, and P. Lightfoot, *J. Solid State Chem.* **122,** 81 (1996).
14. J. De Meulenaer and H. Tompa, *Acta Crystallogr.* **19,** 1014 (1965).
15. G. M. Sheldrick, "SHELXS-86 User Guide," Crystallography Department, University of Göttingen, Göttingen, Germany, 1986.
16. "International Tables for X-Ray Crystallography," Vol. IV. Kynoch Press, Birmingham, 1974.
17. D. T. Cromer and D. Liberman, *J. Chem. Phys.* **531,** 1891 (1970).
18. C. T. Prewitt, "SFLS-5, Report ORNL-TM 305," Oak Ridge National Laboratory, Oak Ridge, TN, 1966.
19. K. Yvon, W. Jeitscho, and E. Parthe, *J. Appl. Crystallogr.* **10,** 73 (1977).
20. G. Malmros, *Acta Chem. Scand.* **24,** 384 (1970).
21. I. D. Brown and D. Altermatt, *Acta Crystallogr., Sect. B: Struct. Sci.* **B41,** 244 (1985).
22. S. C. Nyburg, G. A. Ozin, and J. T. Szymanski, *Acta Crystallogr., Sect. B: Struct. Crystallogr. Cryst. Chem.* **B27,** 2298 (1971).
23. L. G. Sillen, Dissertation, University of Stockholm, Stockholm, 1970.
24. J. F. Ackerman, *J. Solid State Chem.* **62,** 92 (1986).
25. C. J. Milne, P. Lightfoot, J. D. Jorgensen, and S. Short, *J. Mater. Chem.* **5,** 1419 (1995).
26. J. Huang and A. W. Sleight, *J. Solid State Chem.* **96,** 154 (1992).
27. R. D. Shannon, *Acta Crystallogr., Sect. A: Cryst. Phys., Diffr., Theor. Gen. Crystallogr.* **A32,** 751 (1976).
28. W. G. Fateley, F. R. Dollish, N. T. McDewitt, and F. F. Benthey, "Infrared and Raman Selection Rules for Molecular and Lattice Vibrations—Correlation Method." Wiley-Interscience, New York, 1960.
29. P. Tarte, A. Rulmont, and C. Merkaert-Ansay, *Spectrochim. Acta* **42A,** 1009 (1986).
30. Ph. Colomban, *Solid State Ionics* **21,** 97 (1986).
31. A. Mbanza, E. Bores, and P. Courtine, *Mater. Res. Bull.* **20,** 251 (1985).
32. J. M. Winand, A. Rulmont, and P. Tarte, *J. Solid State Chem.* **107,** 356 (1993).
33. M. Barj, H. Perthuis, and P. Colomban, *Solid State Ionics* **9–10,** 845 (1983).
34. C. E. Derrington, A. Lindner, and M. O'Keeffe, *J. Solid State Chem.* **15,** 171 (1975).